Korean J. Chem. Eng., 39(12), 3434-3441 (2022)
DOI: 10.1007/s11814-022-1237-6

pISSN: 0256-1115
eISSN: 1975-7220

Study on temperature characteristics of gasoline engine particulate filters during fuel cut-off

Nan Li*,†, Zheng Nan*, Qiushi Zhang, Haitao Liu**, Lun Hua**, and Caihong Zhang***

*School of Vehicles and Energy, Yanshan University, Qinhuangdao 066004, China
**Suzhou Automotive Research Institute of Tsinghua Univresity, Suzhou 215000, China
(*Received 25 March 2022 • Revised 20 June 2022 • Accepted 19 July 2022*)

Abstract−Based on the bench test of a 1.5 L gasoline engine equipped with a catalytic gasoline engine particulate filter (CGPF), the fuel cut-off regeneration characteristics of the next generation with small pore size GPF and the common GPF under different soot loading and temperatures were studied. The results showed that after the fuel was cut-off during the regeneration process, the center temperature of the sample rose exponentially, and as the regeneration time extended, the temperature gradually became flat. The temperature distribution inside the carrier was such that the inlet temperature was low at the axial position, and the temperature near the outlet was high, the radial position showed a trend of high temperature in the middle and low temperature at the edge, and the temperature difference between the edge and the center of the carrier was large. The maximum temperature inside the GPF increased with the increase in soot loading, and the maximum temperature gradient also increased. When the soot loading reached 6 g/L and the fuel cut-off regeneration was conducted at 650 °C, the maximum and maximum temperature gradient inside the GPF exceeded the tolerance limit of the GPF, and the inside of the carrier was damaged to varying degrees. Therefore, these parameters should be controlled during regeneration.

Keywords: Gasoline Engine Particulate Filter, Fuel Cut-off, Regeneration Characteristics, Temperature Distribution

INTRODUCTION

At present, gasoline direct injection (GDI) engines are widely used worldwide due to their high fuel economy [1-3] However, due to the variable nature of GDI gasoline engines, the incomplete combustion of particulate matter (PM) has caused serious pollution to the environment [4,5]. These particles can enter the human body through the respiratory tract and cause potential health hazards [6, 7]. Since the implementation of China's VI national regulations, strict restrictions have been imposed on the emissions of gasoline engines [8,9]. Therefore, it is necessary to install GPF on gasoline engines to reduce the emissions of particulates [10-14]. Research shows that installing a GPF is highly effective in reducing particulate matter [15,16]. The general GPF filtration efficiency can reach more than 80% [17].

The correct amount of soot in the GPF will increase the filter efficiency of the GPF [18,19]. However, a throttling effect will appear in the exhaust pipe when soot accumulation increases, the exhaust flow resistance will increase and this affects the economy of the engine. Therefore, regeneration and removal of the soot in the GPF should be performed at the appropriate time [20-22]. Active regeneration, passive regeneration and mixed regeneration are the main regeneration methods for removing particulate matter [23-25]. In passive regeneration, when the GPF inlet temperature is sufficient, the fuel cut-off can trigger the regeneration. This regeneration method generally has higher requirements for the GPF inlet temperature and the quantity of soot, and the high temperature thermal shock caused by the high inlet temperature and soot load will damage the sample structure [26-28]. Generally, the highest temperature resistance of the cordierite carrier is below 1,100 °C. With optimization of the GPF structure, the temperature resistance has increased. Regeneration will be prevented when the temperature exceeds the resistance temperature.

Fuel cut-off is a common method of engine regeneration. When the pedal is suddenly released during high-speed driving, the engine gradually decelerates and enters the idle state. At this time, a large amount of air enters the GPF, which causes after-combustion to a certain extent, resulting in a sharp increase in the internal temperature of the GPF, and the small exhaust flow at idle speed cannot dissipate the heat in time. The carrier will suffer a high temperature event in an instant, with the risk of burning the GPF [29].

In addition to this regeneration method, many scholars have also analyzed the regeneration performance of the carrier through various other regeneration methods. [30] developed a fuel cut-off test procedure to determine the maximum temperature by monitoring the internal temperature and temperature gradient of the GPF, and the results showed that the increase in the central temperature of the GPF changed exponentially with the inlet temperature. [31] established a stable soot-oxidation kinetic model, and studied the mechanism of soot-oxidation under normal conditions through acquisition of a large quantity of experimental data and vehicle tests and the results showed that the main passive regeneration mechanism was the fuel cut-off and oxygen supply during the fuel cut-off process. [29], using Printex® U instead of soot to conduct soot oxida-

†To whom correspondence should be addressed.
E-mail: linan@ysu.edu.cn

Table 1. Parameters of the GPF

Name	Diameter	Length	Material	Porosity	Median aperture
GPF-A	118 mm	127 mm	Cordierite	63%	19 μm
GPF-B	118 mm	127 mm	Cordierite	63%	15 μm

Table 2. Engine specifications

Parameters/Units	Parameter value
Fuel injection	Direct injection
Cylinder	3-Cylinder
Intake method	Supercharged
Emission standards	China VI
Post-processing	TWC+GPF
Displacement /L	1.477
Max power (kW)/speed (rpm)	125 kW/5,500 rpm
Max torque (N·m)/speed (rpm)	250/1,500-4,000

Table 3. Main test equipment

Device	Type
Dynamometer	Ht250 HORIBA
Fuel consumption meter	AVL 740
Emission analyzer	MEXA-ONE-D2-EGR
Coolant control system	DET8510
Type-K thermocouple	Φ0.5×700 mm

tion studies under the fuel cut-off, evaluated the effects of variables including fuel cut-off time, soot load, GPF inlet temperature and flow rate on the experimental results. The results showed that higher soot load, higher inlet temperature and a longer oxygen supply cycle led to a higher exotherm. [32] researched diesel particulate filter (DPF) regeneration and found that the inhomogeneity of soot distribution in the DPF directly affects the temperature field distribution during the DPF regeneration. [33] used microwave regeneration to make DPF reach 600 °C within 180 s of microwave start-up. [34] studied the effect of catalyst coating on the regeneration performance of GPF and showed that a uniform coating can improve the soot oxidation rate.

At present, the regeneration of GPF in domestic is mainly about active regeneration, and there is little research on passive regeneration. A large number of fuel-cut regeneration studies are mainly concentrated on the DPF [35,36]. Therefore, this study was performed according to the fuel cut method to study the temperature distribution inside the GPF under different soot loadings and GPF inlet temperatures, which provided a theoretical basis for the safe regeneration of the GPF and the use of the GPF in the future.

EXPERIMENTAL DEVICE AND METHOD

1. Experimental Device

The engine used in this test was a 1.5 L in-line cylinder direct injection supercharged engine, The 1.5 L engine was connected to an electric dynamometer and the dynamometer was controlled by an automation and control system. And the post-processing used was a tightly coupled three-way catalyst (TWC)+GPF. The GPF of the two specification carriers were the same except for the median aperture. The medial aperture of GPF-A was 19 μm, and the median aperture of GPF-B was 15 μm, which is the next generation of high filter efficiency products. According to the information of GPF supplier, the maximum temperature that GPF can withstand is between 1,250-1,300 °C. The parameters of the two GPFS are shown in Table 1. The relevant technical parameters of the engine used are shown in Table 2, and the bench and related test equipment are shown in Table 3.

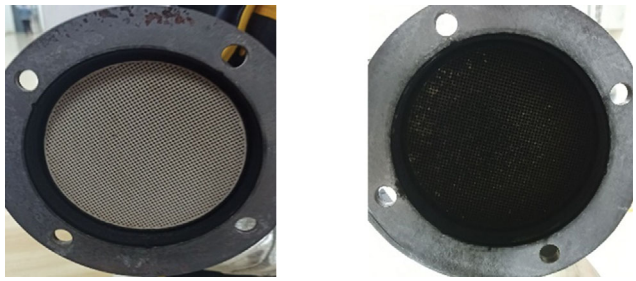

Fig. 1. Contrast of the GPF-B without soot loading and with soot loading.

2. GPF Soot Loading and Thermocouple Distribution

In the experiment, the GPF soot was loaded on the bench by enriching the air-fuel ratio. Under a stable exhaust flow rate of about 95 kg/h, the air-fuel ratio was adjusted to 0.98, and the fuel injection pressure was reduced to make the fuel atomized insufficient, so as to achieve rapid soot loading. In this paper, the GPF and the exhaust pipe are connected by a reducing diameter, which acts as a transition section. This shape makes more soot deposition in the central area of GPF and gradually reduce to the edge. During the test, in the fuel cut-off stage, the electric dynamometer was used to drag the engine backwards to control the speed to idle speed, and in the idle stage, the fuel injection of the engine was restored to make the engine run at a stable idle speed. Fig. 1 shows the comparison of the GPF before and after soot loading. The mass before and after soot loading was weighed with a high precision electronic scale, and the error of soot was ±0.3 g. Before weighing, the GPF was placed in a muffle furnace and kept at 250 °C for 1-2 h to avoid quality errors caused by temperatures differences.

Due to the uneven distribution of soot inside the GPF, the temperature distribution at each position inside the GPF was also different. In order to study the temperature distribution at different positions, it was necessary to arrange multiple thermocouples in the radial and axial positions inside the GPF. The layout of the measuring points, number and distance of each measuring point of the thermocouples in this test is shown in Fig. 2. Because the GPF was axisymmetric, it was only necessary to measure on one side, and seven thermocouples were arranged on the radial end face, with a

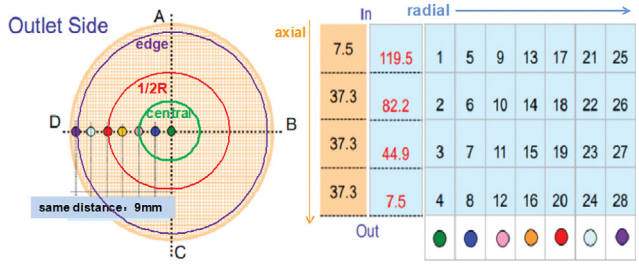

Fig. 2. Distribution of thermocouples in the GPF.

Table 4. Experimental conditions for the regeneration tests

Soot amount		2 g/L	3 g/L	4 g/L	6 g/L
		√ GPF A; √ GPF B			
Temp.	600 °C		√√	√√	√√
	650 °C		√√	√	√√
	700 °C	√√		√√	

distance of 9 mm between them. Four thermocouples were arranged on the axial end face, the first end face was 7.5 mm away from the end face of the GPF inlet, and the other end faces were arranged at an equal distance of 37.3 mm from the previous end face.

The fuel cut-off regeneration characteristics of the two carriers were compared under different soot loading and GPF inlet temperatures, and the performance difference of the GPF was judged by studying the change in the internal temperature of the GPF in the fuel cut-off under different soot loading and the maximum soot loading limit. By controlling the GPF inlet temperature, the distribution law of the maximum temperature and temperature gradient that may occur inside the GPF was further analyzed. It provided a reference for the subsequent study of the GPF temperature distribution and regeneration temperature optimization. The test conditions are shown in Table 4.

3. Test Process

The test process is shown in Fig. 3. Before the test, the engine was preheated. In the first stage, the preheating speed was 1,500 rpm, the engine load was 18%, and the air-fuel ratio was 1.0. After preheating for a period of time, the oil temperature and circulating water temperature reached the heat engine temperature, then the speed was set to 2,000 rpm, the engine load was adjusted to 21%, the air-fuel ratio was held unchanged for three min, and the GPF front temperature was maintained at about 500 °C. Then the engine speed was increased to 3,500 rpm, by increasing the fuel injection, the GPF inlet temperature reached the corresponding target temperature, and the air-fuel ratio was set to 0.98 to prevent the soot from reacting. When the temperature reached the target temperature, the engine fuel was cut-off by controlling the engine control unit (ECU). At the moment of fuel cut-off, a large amount of air entered the GPF. Due to the high internal temperature of the GPF, the soot burned rapidly, and the temperature inside the GPF rose rapidly. After the engine decelerated to the idle speed, the fuel supply was restored, and the air-fuel ratio adjusted to 1.0, and maintained for a period of time under the idle speed condition. After the temperature of the GPF was lowered, the test was terminated, and then the GPF was removed for insulation and weighing, and the mass of the soot involved in the reaction was calculated.

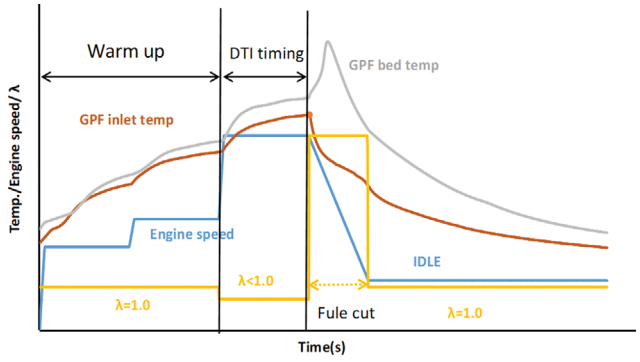

Fig. 3. Schematic diagram of the test process.

RESULTS AND DISCUSSION

1. Soot Loadings

Fig. 4 shows the change of pressure drop of GPF B during accumulation of soot. At the initial stage of soot accumulate, soot is mainly deposited in the pores of GPF wall, result the pressure drop increases rapidly, which is called deep bed capture. The build-up of soot at this stage has a big impact on the pressure drop, and the pressure drop does not increase linearly as a function of accumulation soot. The filter cake layer capture is dominant with the increase of soot accumulation. The response of GPF pressure drop to soot will be more linear. During the steady-state accumulation of soot, the average soot generation rate measured by the smoke meter is about 0.37 mg/s.

2. Regeneration Performance under Different Soot Loadings

Fig. 5 shows the maximum temperature inside the carrier during fuel cut-off tests at different soot loadings. Fig. 5 shows that under the same soot loading, when the soot loading was <6 g/L, the maximum temperature inside the GPF A was lower than that of the GPF B. When the soot loading reached 6 g/L, the maximum temperature of GPF A exceeded that of GPF B after the fuel cut-off. The main reason was that when the soot loading was small, the deposition of soot was trapped in the deep bed filter. Since the

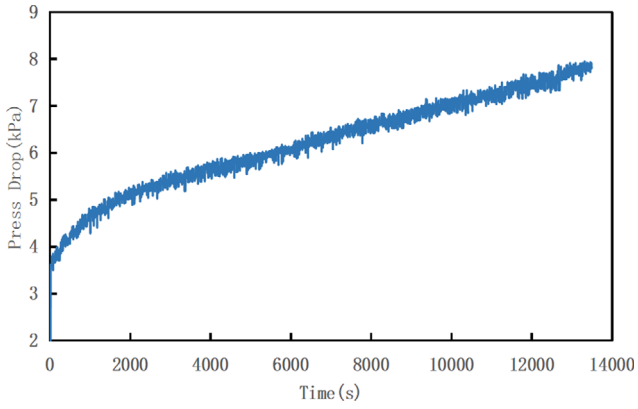

Fig. 4. Variation of GPF B pressure drop with soot accumulation.

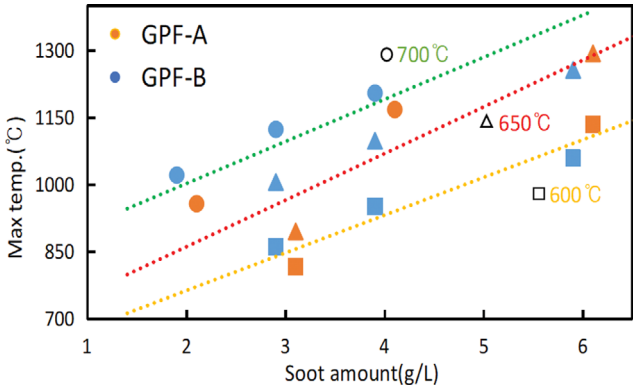

Fig. 5. Variation of the maximum temperature inside the GPF when the fuel was cut-off under different soot loads.

median pore size of GPF B was small, more soot was carried per unit volume in the pores of GPF B. After the fuel was cut-off, a large amount of air entered and caused post-combustion, and the soot burned rapidly under high temperature and oxygen-rich conditions, resulting in a higher temperature for GPF B. When the soot load gradually increased, the soot deposition changed from the initial deep bed filter to the soot layer filter. At that time, the soot in the pore size of the GPF was saturated. Since the pore size of GPF A was larger, the total amount of soot in the pores was large, resulting in a higher temperature of soot combustion after fuel cut at high soot loads.

When the fuel was cut off at the same inlet temperature, the maximum temperature inside the GPF increased with the increase in soot loading, and the increase in soot loading by 1 g/L produced a temperature rise of about 100 °C. Fig. 5 shows that when the fuel was cut off at the same temperature, the maximum temperature under different soot loads showed a good linear relationship. Therefore, before the fuel was cut off, it was necessary to pay attention to the temperature at the time of the fuel cut-off and the amount of soot inside the GPF to prevent the GPF from being burnt out by high temperature due to the high amount of soot or high inlet temperature.

3. The GPF Internal Temperature Distribution when the Fuel was Cut-off at the Soot Load of 6 g/L and the Inlet Temperature at 650 °C

In Fig. 5, the peak temperature generated by GPF is higher under the regeneration condition of 6 g/L and 650 °C, so this condition is selected to analyze the temperature change inside GPF during regeneration. Fig. 6 shows the change in the internal temperature of the GPF after the fuel cut-off. Fig. 6 shows that the temperature inside the two carriers increased in a controlled manner before the fuel was cut-off. At the moment of fuel cut-off, a large amount of air quickly entered the inside of the GPF. At this time, the temperature had reached the temperature required for soot combustion. Therefore, the internal temperature of the GPF showed an uncontrollable exponential increase, after reaching the peak temperature, due to the decrease in the amount of soot inside the GPF, the temperature showed an exponential downward trend, and the temperature inside the GPF gradually becomes flat after a period of time. During this period, the maximum temperature of GPF A reached

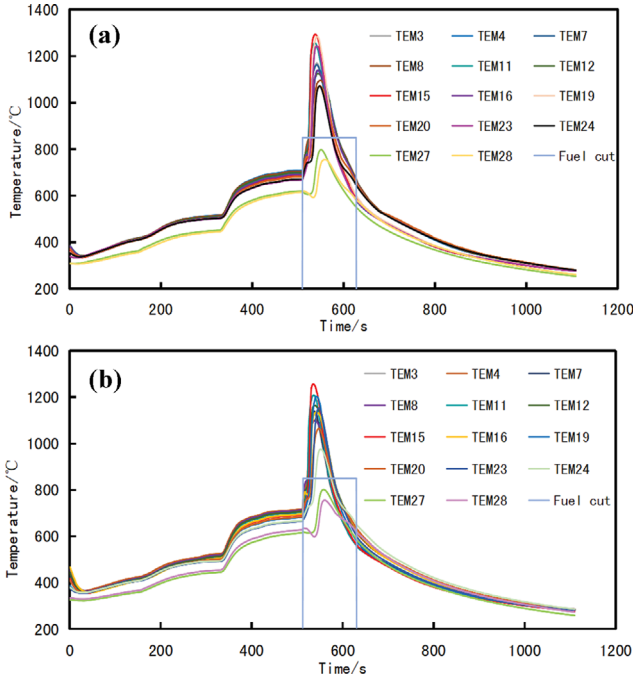

Fig. 6. Internal temperature of two carriers with soot loading of 6 g/L. (a) GPF A, (b) GPF B.

1,293.8 °C at point 15, and the maximum radial temperature gradient appeared between points 27 and 23, reaching as high as 602.9 °C/cm. The highest temperature of GPF B also appeared at point 15, the peak temperature reached 1,256.8 °C, and the maximum radial temperature gradient also appeared between measuring points 27 and 23, reaching 461.7 °C/cm. Fig. 6 shows that the temperature at the edge of the GPF was lower (for instance measuring points 20-28), and there was no obvious temperature peak during regeneration. The main reason was that during the soot loading process, due to the effect of the airflow, the central and 1/2R of the carrier was loaded with more soot, and the reaction at the central was more intense during regeneration, while the amount of soot loaded on the edge part was less, and the edge part was directly connected to the atmosphere during regeneration, resulting in faster heat dissipation. Therefore, the central of the GPF was more likely to generate the highest temperature, which also led to a large temperature gradient between the edge part and the central of the GPF.

4. The Temperature Field Distribution of the GPF Space when the Fuel is Cut Off under the Soot Load is 6 g/L and the Inlet Temperature at 650 °C

After the fuel cut-off, the temperature field inside the GPF showed that the center temperature was higher than the edge, the outlet temperature was higher than the inlet temperature, and the center near the outlet had the highest temperature, which was mainly due to the deposition of soot in the center. After the regeneration was triggered, the heat generated by the combustion of the soot would be transferred to the end of the GPF with the exhaust gas flow. Due to the reduced engine speed, the exhaust gas flow was small and the heat could not be quickly discharged, thus forming a heat accumulation at the rear end of the GPF, and the heat dissipation at the center was not as rapid as at the edges, so the position of the GPF

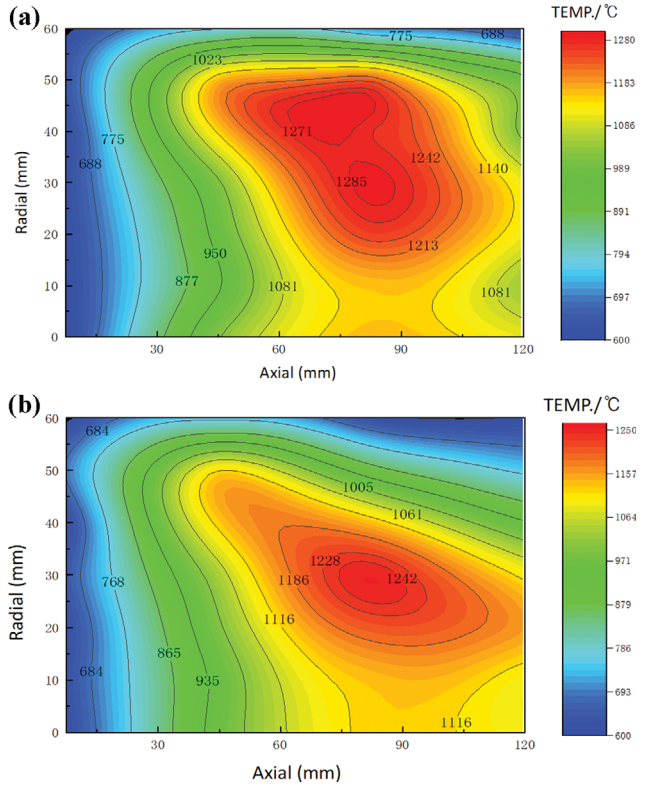

Fig. 7. Internal temperature field the carriers with soot loading of 6 g/L. (a) GPF A, (b) GPF B.

close to the outlet was more likely to generate a higher temperature. Taking the soot loading of 6 g/L as an example, the distribution of the internal temperature field of the GPF at the moment of the highest temperature of the two carriers was compared.

Fig. 7 shows the temperature distribution of the axial and radial positions of the GPF during regeneration at 650 °C when the soot loading was 6 g/L. In the axial direction, the temperature at the inlet of GPF was lower, and the middle and near the outlets were higher. In the radial position, the temperature was high at the 1/2R position, and the closer to the edge, the lower the temperature.

5. The Effect of Soot Loading on the Maximum Temperature Gradient of the GPF

When considering whether the GPF can be safely regenerated under the corresponding soot loading, it mainly depended on whether the maximum temperature inside the GPF exceeded the maximum temperature limit. In addition, the maximum temperature gradient of the GPF was also one of the main influencing factors. Through the analysis of the internal temperature field of the GPF, it was found that a larger temperature gradient would be generated at the edge of the GPF, so the differences in the temperature gradient of the two carriers at different regeneration temperatures were compared and analyzed.

Fig. 8 shows that with the increase in soot loading, the maximum temperature gradient also increased. At the same time, the increase in the inlet regeneration temperature also led to an increase in the temperature gradient. In the test, the maximum temperature gradient of the GPF mostly occurred between measuring points 27

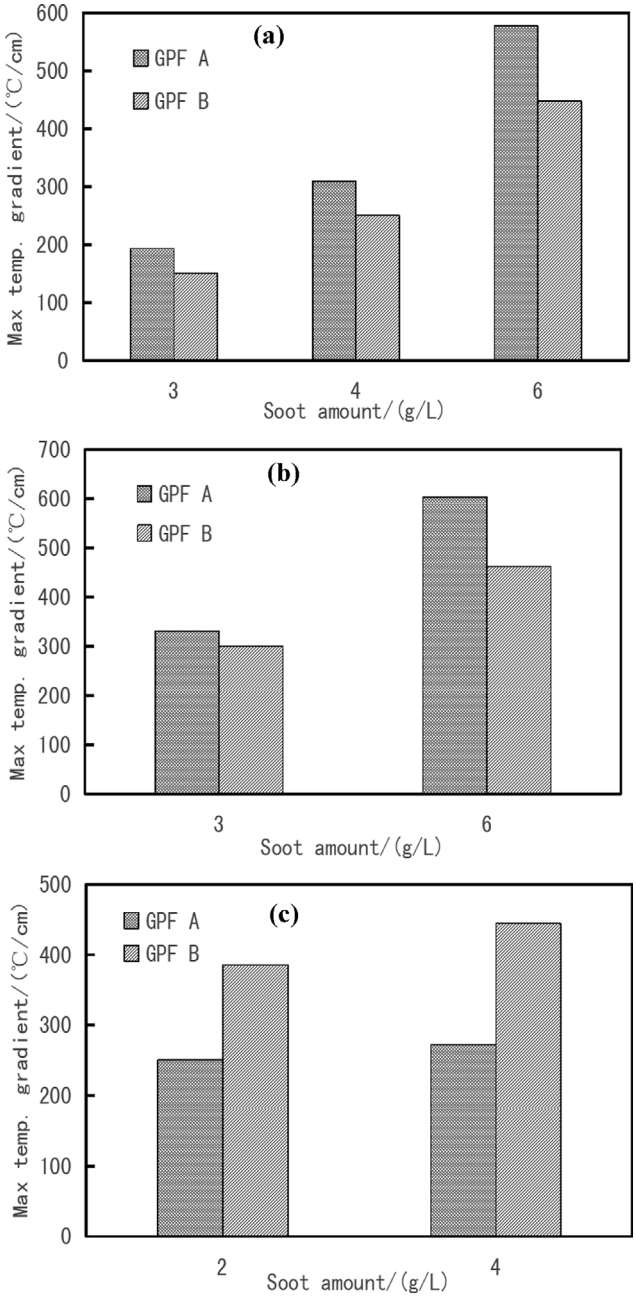

Fig. 8. Maximum temperature gradient in the regeneration process. (a) Inlet temperature at 600 °C, (b) Inlet temperature at 650 °C, (c) Inlet temperature at 700 °C.

and 23, and between measuring points 28 and 24. When the inlet temperature was 600 °C and 650 °C, the temperature gradient of GPF A was higher than that of GPF B. When the inlet temperature was 700 °C, the temperature gradient of GPF B was higher than that of GPF A, and the difference between the two carriers increased slightly with the increase soot loading. This is because the greater the soot load, the more intense the reaction and the higher the temperature, resulting in the greater difference of temperature gradient. When the inlet temperature was 600 °C and 650 °C, the maximum temperature gradient of GPF A reached 577.2 °C/cm and 602.9 °C/cm respectively, which exceeded the temperature gradient limit of

Table 5. CT equipment parameters

Equipment type	NSI X5000
Tube voltage range /kv	10-450
Minimum focus size /nm	<500
Detector Max. size /cm	40×40
External dimensions /cm	200×274×232
Scan stroke /cm	Vertical: 122 cm; level: 84 cm; Z-axis: 122 cm
Bearing weight /kg	90

the GPF. During regeneration process, the GPF is easy to be damaged due to the large temperature gradient between the edge and the interior of GPF. Therefore, attention should be paid to the position of the edge.

CT SCAN RESULTS

Before starting the test, scan the new GPF to confirm that there is no damage and then carry out the test. When the maximum temperature of the GPF exceeded 1,200 °C, CT scan was performed after the test. After the fuel cut-off regeneration with the soot loading of 6 g/L and a regeneration temperature of 650 °C, the peak temperatures of both GPFs exceeded the structural damage limit temperature of the carrier, and the maximum radial temperature gradient of GPF A far exceeded that which the cordierite sample could withstand. Therefore, after the regeneration condition was over, a CT scan was performed on the inside of the GPF to determine whether the internal structure of the carrier was damaged.

The CT scan equipment model was NSI X5000. It was high resolution digital multi-axis X-ray imaging equipment. At present, it was mostly used to scan the internal structure of the GPF [37,38]. The equipment works by taking hundreds or thousands of 2D Digital Radiography projections around a 360° rotation of an object. Proprietary algorithms are then used to reconstruct the 2D projections into a 3D CT volume, which will allow you to view and slice the part at any angle. The interior of parts of various shapes, sizes, and weights could be inspected. The main parameters of the equipment are shown in Table 5.

The full-scale nondestructive scanning of GPF was performed,

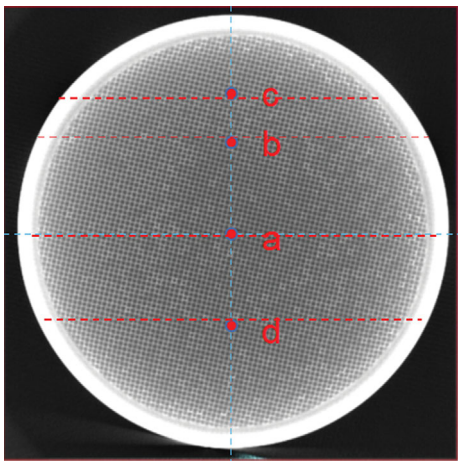

Fig. 9. GPF section CT results.

and the scanning results of the two carriers are shown in Fig. 9-Fig. 11. It is the cross section cut from the four points of GPF a, b, c and d along the dotted line. Fig. 9 shows that there were obvious cracks near the outlet of GPF A. Because the exhaust gas flow brought a lot of heat to the outlet and discharged it, the outlet was more likely to be damaged. At the same time, the closer to the edge of the GPF, the more serious the damage. Under this condition, the maximum temperature of GPF B for fuel cut-off regeneration also exceeded the GPF tolerance limit. From the section d, a slight crack was found near the outlet of the GPF. It can be seen that the degree of damage to GPF B was lower than that to GPF A, so GPF B had better ability to withstand high temperature impact. Under the soot load-

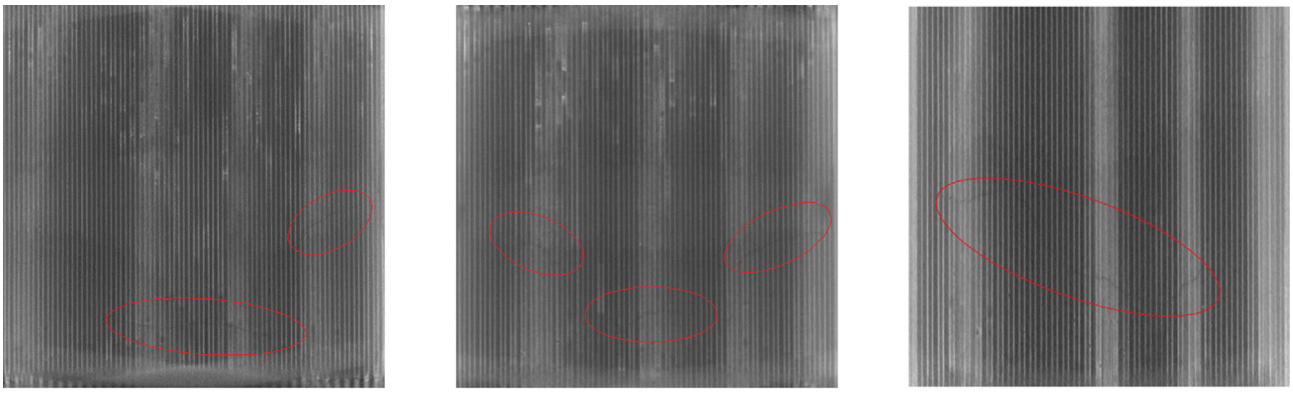

(a) (b) (c)

Fig. 10. CT scanned filters of GPF A. (a) Section a, (b) Section b, (c) Section c.

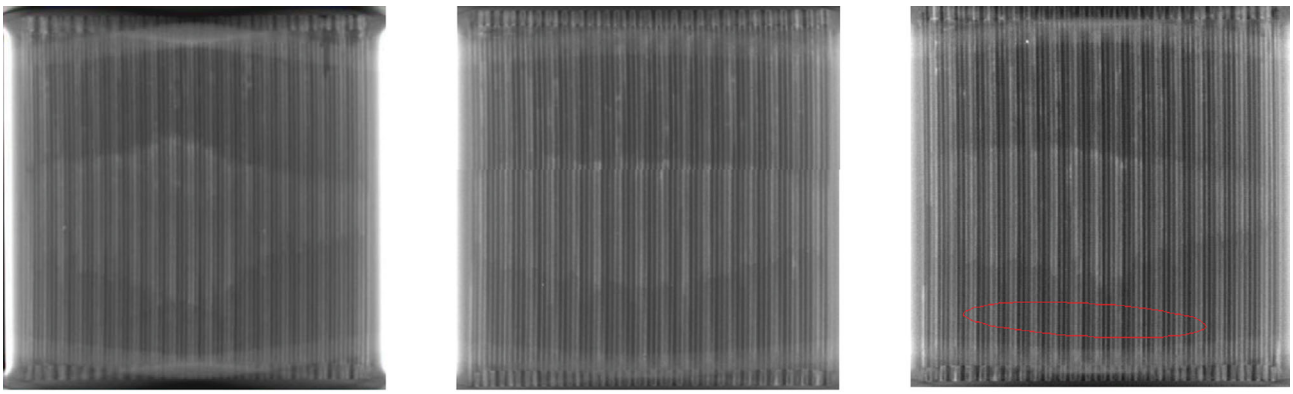

Fig. 11. CT scanned filters of GPF B. (a) Section a, (b) Section b, (c) Section d.

ing of 6 g/L, and the inlet temperature of 650 °C, the GPF should be avoided as much as possible to prevent the carrier from being damaged.

CONCLUSIONS

(1) When the fuel was cut-off, the higher soot load and the higher inlet temperature led to a higher maximum temperature inside the GPF, and the maximum temperature gradient increased accordingly. In addition, the test found that the peak temperature inside the GPF would increase by about 100 °C for every 1 g/l of soot added under the same working conditions.

(2) After the fuel cut-off, the temperature first rose exponentially and rapidly, with the continuous combustion of PM. The temperature gradually decreased and leveled-off. During this period, the highest temperature inside the GPF mostly occurred at the radius of 1/2R, which was close to the middle and rear sections of the GPF. In the axial position, the inlet temperature was low, the temperature near the outlet was high. The radial temperature was higher near the center, and the temperature gradually decreased near the edge of the GPF. The maximum temperature gradient appeared near the edge of the carrier.

(3) When the fuel was cut-off at the soot load of 6 g/L and the inlet temperature was 650 °C, the maximum temperature inside GPF A and GPF B were 1,293.8 °C and 1,256.8 °C, respectively, both exceeding the temperature tolerance limit of the GPF. After CT scanning, it was found that GPF A was obviously cracks in many places, while GPF B had only slight cracks. In general, GPF B had better safe regeneration performance. For safety, when the soot loading exceeds 6 g/L and the GPF inlet temperature exceeds 650 °C, the oil cut-off regeneration shall be prohibited as far as possible. When the GPF was cracks, it should be replaced a new GPF in time, otherwise particles would escape through the cracks, affecting the collection of dust, resulting in excessive emission of particles.

STATEMENTS AND DECLARATIONS

Ethics Declarations

The paper does not involve relevant ethical research.

Consent to Participate

I am free to contact any of the people involved in the research to seek further clarification and information.

Consent to Publish

All the authors listed have approved the manuscript that is enclosed.

Author Contributions

All authors contributed to the study conception and design. Material preparation, data collection and analysis were performed by Qiushi Zhang, Haitao Liu, Lun Hua and Caihong Zhang. The first draft of the manuscript was written by Nan Li and Zheng Nan and all authors commented on previous versions of the manuscript. All authors read and approved the final manuscript.

Funding

This work was supported by Natural Science Foundation of Hebei Province (Grant numbers E2019203527).

Competing Interests

The authors have no relevant financial or non-financial interests to disclose.

Availability of Data and Materials

The datasets used and/or analyzed during the current study are available from the corresponding author on reasonable request.

REFERENCES

1. A. Mamakos, G. Martini, A. Marotta and U. Manfredi, *J. Aerosol Sci.*, **63**, 115 (2013).
2. C. Gong, X. Si and F. Liu, *Fuel*, **303**, 121262 (2021).
3. X. Liu, T. Chanko, C. Lambert and M. Maricq, *SAE Int. Technical Paper*, 2018-01-1259 (2018).
4. J. Du, W. C. Sun, L. Guo, S. L. Xiao, M. Z. Tan, G. L. Li and L. Y. Fan, *Energy Convers. Manage.*, **100**, 300 (2015).
5. W. J. Zhong, T. M. Xuan, Z. X. He, Q. Wang, D. Li, X. Zhang and Y. Y. Huang, *Energy Convers. Manage.*, **121**, 241 (2016).

6. B. Liang, Y. S. Ge, J. W. Tan, X. K. Han, L. P. Gao, L. J. Hao, W. T. Ye and P. P. Dai, *J. Aerosol Sci.*, **57**, 21 (2013).
7. M. M. Zhang, W. Hong, F. X. Xie, Y. Su, H. T. Liu and S. T. Zhou, *Energy Convers. Manage.*, **164**, 344 (2018).
8. J. Y. Ko, K. J. Kim, W. Y. Chung, C. L. Myung and S. Park, *Fuel*, **238**, 363 (2019).
9. F. Bonatesta, E. Chiappetta and L. Rocca, *Appl. Energy*, **124**, 366 (2014).
10. W. J. Zhong, P. Tamilselvan, Q. Wang, Z. X. He, H. Feng and X. Yu, *Energy*, **153**, 349 (2018).
11. E. Distaso, R. Amirante, P. Tamburrano and D. Reite, *Energy Convers. Manage.*, **184**, 24 (2019).
12. J. J. Wang, F. W. Yan, N. Fang, D. Yan, G. Q. Zhang, Y. Wang and W. L. Yang, *Energies*, **13**, 1 (2020).
13. F. X. Xie, W. Hong, Y. Su, M. M. Zhang and B. P. Jiang, *Energy Convers. Manage.*, **142**, 69 (2017).
14. S. Choi, K. Oh and C. Lee, *Energy*, **77**, 327 (2014).
15. P. Piqueras, E. Sanchis, J. Herreros and A. Tsolakis, *Chem. Eng. Sci.*, **234**, 116437 (2021).
16. C. Saito, T. Nakatani, Y. Miyairi, K. Yuuki and C. Vogt, *SAE Technical Paper*, 2011-01-0814 (2011).
17. H. Badshah, D. Kittelson and W. Northrop, *SAE Int. J. Engines*, **9**, 1775 (2016).
18. P. Tandon, A. Heibel, J. Whitmore, N. Kekre and K. Chithapragada, *Chem. Eng. Sci.*, **65**, 4715 (2010).
19. Z. W. Meng, Z. Chen, J. Tan, W. Wang, Z. L. Zhan, J. F. Huang and J. Fang, *Chem. Eng. Sci.*, **248**, 117114 (2022).
20. T. Chan, M. Saffaripour, F. S. Liu, J. Hendren, K. Thomson, J. Kubsh, R. Brezny and G. Rideout, *Emission Control Sci. Technol.*, **2**, 75 (2016).
21. Q. S. Zuo, Y. Y. Tang, W. Chen, J. P. Zhang, L. Shi and Y. Xie, *Fuel*, **265**, 117001 (2020).
22. V. Bermudez, J. R. Serrano, P. Piqueras and O. Garcia, *Appl. Energy*, **140**, 234 (2015).
23. G. Landi, V. Sarli and L. Lisi, *Topics Catal.*, **64**, 270 (2021).
24. V. Palma and E. Meloni, *Fuel*, **181**, 421 (2016).
25. Z. Stępień, L. Ziemiański, G. Żak, M. Wojtasik, L. Jeczmionek and Z. Burnus, *Fuel*, **161**, 278 (2015).
26. V. D. Sarli and A. D. Benedetto, *AIChE J.*, **64**, 1714 (2018).
27. V. D. Sarli, G. Landi, A. D. Benedetto and L. Lisi, *Topics Catal.*, **64**, 256 (2021).
28. S. Soltani, R. Andersson and B. Andersson, *Fuel*, **220**, 453 (2018).
29. T. Boger, D. Rose, P. Nicolin, N. Gunasekaran and T. Glasson, *Emission Control Sci. Technol.*, **1**, 49 (2015).
30. X. Feng, H. Liu, W. Li, S. He and Z. Lu, *SAE Technical Paper*, 2019-01-0968 (2019).
31. P. Nicolin, D. Rose, F. Kunath and T. Boger, *SAE Int. J. Engines*, **8**, 1253 (2015).
32. A. G. Konstandopoulos, M. Kostoglou and P. Housiada, *SAE Technical Paper*, **110**, 609 (2001).
33. C. Kurien, A. K. Srivastava, N. Gandigudi and K. Anand, *J. Energy Inst.*, **93**, 463 (2020).
34. I. Belot, D. Vidal, R. Greiner, M. Votsmeier, R. E. Hayes and F. Bertrand, *Chem. Eng. J.*, **406**, 127040 (2021).
35. J. Benajes, A. García, J. Monsalve-Serrano, I. Balloul and G. Pradel, *Energy Convers. Manage.*, **123**, 381 (2016).
36. Z. W. Meng, C. Chen, J. S. Li, J. Fang, J. Tan, Y. Qin, Y. Jiang, Z. H. Qin, W. L. Bai and K. Liang, *Fuel*, **262**, 116589 (2020).
37. J. Gong, M. L. Stewart, A. Zelenyuk, A. Strzelec, S. Viswanathan, D. A. Rothamer, D. E. Foster and C. J. Rutland, *Chem. Eng. J.*, **338**, 15 (2018).
38. H. Nakayama, Y. Banno, H. Mochizuki, H. Hara, A. Takayama, M. Nagata, Y. Sasaki and S. Yoneyama, *Topics Catal.*, **62**, 419 (2019).